Journal of Molecular Structure 1155 (2018) 403–413

Contents lists available at ScienceDirect

Journal of Molecular Structure

journal homepage: http://www.elsevier.com/locate/molstruc

Synthesis, crystal structures, computational studies and antimicrobial activity of new designed bis((5-aryl-1,3,4-oxadiazol-2-yl)thio)alkanes

Muhammad Naeem Ahmed [a, *], Beenish Sadiq [a], Najim A. Al-Masoudi [b, **], Khawaja Ansar Yasin [a], Shahid Hameed [c], Tariq Mahmood [d], Khurshid Ayub [d], Muhammad Nawaz Tahir [e]

[a] Department of Chemistry, The University of Azad Jammu & Kashmir, Muzaffarabad 13100, Pakistan
[b] Department of Chemistry, College of Science, University of Basrah, Basrah, Iraq
[c] Department of Chemistry, Quaid-i-Azam University, Islamabad, Pakistan
[d] Department of Chemistry, COMSATS Institute of Information Technology, University Road, Tobe Camp, 22060 Abbottabad, Pakistan
[e] Department of Physics, University of Sargodha, Sargodha Pakistan

ARTICLE INFO

Article history:
Received 26 July 2017
Received in revised form
2 November 2017
Accepted 4 November 2017
Available online 8 November 2017

Keywords:
Antimicrobial activity
Crystal structures
Computational studies
1,3,4-Oxadiazole derivatives

ABSTRACT

A new series of bis((5-aryl-1,3,4-oxadiazol-2-yl)thio)alkanes **4**–**14** have been synthesized *via* nucleophilic substitution reaction of dihaloalkanes with respective 1,3,4-oxadiazole-2-thiols **3a-f**, and characterized by spectroscopic techniques. The structures of **4** and **12** were unambiguously confirmed by single-crystal X-ray diffraction analysis. Density functional theory calculations at B3LYP/6-31 + G(d) level of theory were performed for comparison of X-ray geometric parameters, molecular electrostatic potential (MEP) and frontier molecular orbital analyses of synthesized compounds. MEP analysis revealed that these compounds are nucleophilic in nature. Frontier molecular orbitals (FMOs) analysis of **4**–**14** was performed for evaluation of kinetic stability. All synthesized compounds were screened *in vitro* for antimicrobial activity against three bacterial and three fungal strains and showed promising results.

1. Introduction

1,3,4-Oxadiazole ring serve as important pharmacodynamic nuclei [1,2], and their incorporation in different heterocyclic scaffolds results in various biological activities such as anticancer [3–5], anti-inflammatory [6], hyperglycemic [7], antifungal, antibacterial [8–10], antihypertensive [11], anticonvulsant [12,13], antianalgesic [14], antihepatitis virus B (HBV) [15], and *anti*-HIV agents [16–18] (*e.g.*: Raltegravir, 2-((2-(2-methyl-5-nitro-1*H*-imidazole-1-yl)ethyl)thio)-5-(2-nitrophenyl)-1,3,4-oxadiazole (**1**) [19])) as well as enzyme inhibitors [20–22]. Qian-Ru *et al.* [23] have synthesized 1,3,4-oxadiazole thioether analogues with evaluation of their thymidylate synthase (TS) and anticancer activities. Among all the designed compounds, compound **1** bearing a nitro group showed more remarkable anticancer activity towards *in vitro* three cancer cell lines, which was superior to the positive control. Furthermore, Zhu *et al.* [24] designed a series of 2-(benzylthio)-5-aryloxadiazole derivatives and evaluated for cytotoxicity properties and epidermal growth factor receptor (EGFR) inhibitory activity, where 2-(2-aminophenyl)-5-(benzylthio)-1,3,4-oxadiazole showed the most potent biological activity ((IC_{50} = 1.09 μM for breast adenocarcinoma cell line (MCF-7) and IC_{50} = 1.51 μM for EGFR) with gefitinib as a standard. In 2009, we synthesized a series of adamantylthiazolyl-1,3,4-oxadiazole derivatives where some of these analogues exhibited remarkable anticancer activity against a panel of human cell lines [25]. Macaev *et al.* [26] have reported the biological activity of 5-aryl-2-thio-1,3,4-oxadiazole derivatives against Mycobacterium tuberculosis H37Rv, which some exhibiting more than 90% inhibition of mycobacterial growth at concentration of 12.5 μg/ml.

Based on all above considerations and in continuation of our ongoing work on the development of new 1,3,4-oxadiazole analogues as antimicrobial agents, we report here the synthesis of new bis((5-aryl-1,3,4-oxadiazol-2-yl)thio)alkanes with anticipated antimicrobial activities, by clubbing 1,3,4-oxadiazol with thiomethylene groups as spacers in one frame work. The new analogues

* Corresponding author.
** Corresponding author.
E-mail addresses: aromatics790@gmail.com (M.N. Ahmed), najim.al-masoudi@gmx.de (N.A. Al-Masoudi).
URL: http://www.al-masoudi.de

https://doi.org/10.1016/j.molstruc.2017.11.011
0022-2860/

have been theoretically investigated by applying density functional theory (DFT) to understand the structure activity relationship.

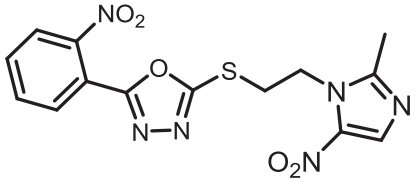

1. Raltegravir, 2-((2-(2-methyl-5-nitro-1*H*-imidazol-1-yl) ethyl)thio)-5-(2-nitrophenyl)-1,3,4-oxadiazole

2. Experimental section

Melting points were determined on a Yanaco melting point apparatus and are reported as uncorrected. FT-IR spectra were recorded on a Nicolet FT-IR 5DX spectrometer using the KBr technique.^{1}H NMR (400 MHz) and ^{13}C NMR (75.5 MHz) spectra were measured on a JEOL-ECA instrument in $CDCl_3$ as solvent and TMS as internal standard. Elemental analysis was carried out using elementar Analysen systeme GmbH - vario EL III Element Analyzer. The reaction progress was monitored by thin layer chromatography (TLC). Column chromatography was performed using a flash column. Benzohydrazide (**2a**), 4-toluic acid hydrazide (**2c**), and 2-Chloro-, 2-bromobenzohydrazides (**2e** and **2f**) were purchased from Sigma Aldrich and TCI (Germany), whereas isonicotinic acid hydrazide (**2b**) [27] and 5-aryl-1,3,4-oxadiazole-2-thiols **3a-e** [28] were prepared according to the literature methods.

2.1. General procedure for the synthesis of bis((5-aryl-1,3,4-oxadiazol-2-yl)thio)alkanes (**4**–**14**)

Dibromoalkane (1.0 mmol) was added to a suspension of 5-aryl-1,3,4-oxadiazole-2-thiols **3a-e** (2.0 mmol) and K_2CO_3 (2.0 mmol) in acetone (20 ml) and the reaction mixture was stirred at 50 °C for 4 h. After reaction completion, the mixture was concentrated, diluted with water (20 ml) and extracted with CH_2Cl_2 (3 × 20 ml) and finally washed with brine. The organic layers was dried (Na_2SO_4), filtered and evaporated to dryness. The residue was purified on a flash column chromatography, using EtOAc-hexane 3:2) as eluent to give the desired product.

For atom numbering refer to Scheme 1.

2.1.1. 1,3-Bis((5-phenyl-1,3,4-oxadiazol-2-yl)thio)propane (**4**)

From dibromopropane (202 mg) and **3a** (356 mg). Yield: 634 mg (80%) as white solid; mp: 109–110 °C; IR (KBr, cm^{-1}): ν_{max} 3055 (CH–Ar), 1592 (C=N), 1463 (C–H bending), 1054 (C–*O*–C oxadiazole); ^{1}H NMR (400 MHz, $CDCl_3$): δ 8.04–8.00 (m, 4H, ArH), 7.57–7.28 (m, 6H, ArH), 3.50 (t, 4H, J = 6.9 Hz, CH_2-a+CH_2-a'), 2.50 (m, 2H, J = 6.9 Hz, CH_2-b); ^{13}C NMR (400 MHz, $CDCl_3$): δ 165.9 ($C_{oxadiazol}$-5+$C_{oxadiazol}$-5′), 163.8 ($C_{oxadiazol}$-2+$C_{oxadiazol}$-2′), 131.7, 129.0, 126.7, 123.5 ($C_{arom.}$), 30.9 (*C*a + *C*a'), 28.7 (*C*b). Elemental analysis calcd for $C_{19}H_{16}N_4O_2S_2$ (396.49) C, 57.56; H, 4.07; N, 14.13, found: C, 57.50; H, 4.01; N, 14.10.

2.1.2. 1,5-Bis((5-phenyl-1,3,4-oxadiazol-2-yl)thio)pentane (**5**)

From dibromopentane (230 mg) and **3a** (356 mg). Yield: 695 mg (82%) as white solid; mp: 118–120 °C; IR (KBr, cm^{-1}): ν_{max} 3055 (CH–Ar), 1592 (C=N), 1463 (C–H bending), 1054 (C–*O*–C oxadiazole); ^{1}H NMR (400 MHz, $CDCl_3$): δ 8.04–8.00 (m, 4H, Ar), 7.54–7.47 (m, 6H, ArH), 3.34 (t, 4H, J = 6.8 Hz, CH_2-a+CH_2-a'), 1.95 (m, 4H, CH_2-b + CH_2-b'), 1.70 (m, 2H, CH_2-c); ^{13}C NMR (400 MHz, $CDCl_3$): δ 165.9 ($C_{oxadiazol}$-5+$C_{oxadiazol}$-5′), 163.7 ($C_{oxadiazol}$-2+$C_{oxadiazol}$-2′), 129.2, 128.7, 127.7, 126.1 ($C_{arom.}$), 36.4 (*C*a + *C*a'), 29.5 (*C*b + *C*b'), 28.5 (*Cc*). Elemental analysis calcd for $C_{21}H_{20}N_4O_2S_2$ (424.10): C, 59.41; H, 4.75; N, 13.20; S, 15.11, found: C, 59.50; H, 4.68; N, 13.15; S, 15.12.

2.1.3. 1,6-Bis((5-phenyl-1,3,4-oxadiazol-2-yl)thio)hexane (**6**)

From dibromohexane (244 mg) and **3a** (356 mg). Yield: 683 mg (78%) as white solid; mp: 119–121 °C; IR (KBr, cm^{-1}): ν_{max} 3055 (CH–Ar), 1592 (C=N), 1463 (C–H bending), 1054 (C–*O*–C oxadiazole); ^{1}H NMR (400 MHz, $CDCl_3$): δ 8.04–8.00 (m, 4H, ArH), 7.57–7.28 (m, 6H, Ar), 3.50 (t, 4H, J = 6.8 Hz, CH_2-a+CH_2-a'), 1.66 (m, 4H, CH_2-b + CH_2-b'), 1.49 (m, 4H, CH_2-c + CH_2-c')); ^{13}C NMR (400 MHz, $CDCl_3$): δ 165.8 ($C_{oxadiazol}$-5+$C_{oxadiazol}$-5′), 163.9 ($C_{oxadiazol}$-2+$C_{oxadiazol}$-2′), 129.7, 128.8127.5, 126.5 ($C_{arom.}$), 36.4 (*C*a + *C*a'), 30.2 (*C*b + *C*b'), 28.7 (*Cc* + *Cc*'). Elemental analysis calcd for $C_{22}H_{22}N_4O_2S_2$ (438.11): C, 60.25; H, 5.07; N, 12.78; S, 14.62, found: C, 60.21; H, 5.00; N, 12.76; S, 14.60.

2.1.4. 1,8-Bis((5-phenyl-1,3,4-oxadiazol-2-yl)thio)octane (**7**)

From dibromoocatne (272 mg) and **3a** (356 mg). Yield: 700 mg (75%) as white solid; mp: 119–120 °C; IR (KBr, cm^{-1}): ν_{max} 3067 (CH–Ar), 1601 (C=N), 1449 (C–H bending), 1054 (C–*O*–C oxadiazole); ^{1}H NMR (400 MHz, $CDCl_3$): δ 8.03–7.99 (m, 4H, ArH), 7.56–7.46 (m, 6H, ArH), 3.30 (t, 4H, J = 7.2 Hz, CH_2-a+CH_2-a'), 1.90 (m, 4H, CH_2-b + CH_2-b'), 1.70 (m, 4H, CH_2-c + CH_2-c'), 1.39 (m, 4H, CH_2-d + CH_2-d'); ^{13}C NMR (400 MHz, $CDCl_3$): δ 165.6 ($C_{oxadiazol}$-5+$C_{oxadiazol}$-5′), 164.5 ($C_{oxadiazol}$-2+$C_{oxadiazol}$-2′), 131.6, 129.0, 126.6, 123.6 ($C_{arom.}$), 36.5 (*C*a + *C*a'), 32.5 (*C*b + *C*b'), 29.1 (*Cc* + *Cc*'), 28.8 (*C*d + *C*d'). Elemental analysis calcd for $C_{24}H_{26}N_4O_2S_2$ (466.62): C, 61.78; H, 5.62; N, 12.01, found: C, 61.70; H, 5.60; N, 11.89.

2.1.5. 1,3-Bis((5-(pyridin-4-yl)-1,3,4-oxadiazol-2-yl)thio)propane (**8**)

From dibromopropane (202 mg) and **3b** (358 mg). Yield: 574 mg (72%) as white solid; mp: 113–115 °C; IR (KBr, cm^{-1}): ν_{max} 3065 (CH–Ar), 1611 (C=N), 1453 (C–H bending), 1054 (C–*O*–C oxadiazole); ^{1}H NMR (400 MHz, $CDCl_3$): δ 8.70 (d, 4H, J = 3.8 Hz, $H_{pyridin}$-2+$H_{pyridin}$-2'+ $H_{pyridin}$-6'+ $H_{pyridin}$-6), 7.91 (d, 4H, J = 3.8 Hz, $H_{pyridin}$-3'+ $H_{pyridin}$-3'+ $H_{pyridin}$-5'+ $H_{pyridin}$-5′), 3.50 (t, 4H, J = 6.9 Hz, CH_2-a+CH_2-a'), 2.46 (quin, 1H, J = 6.9 Hz, CH_2-b),; ^{13}C NMR (400 MHz, $CDCl_3$): δ 166.0 ($C_{oxadiazol}$-5+$C_{oxadiazol}$-5′), 163.4 ($C_{oxadiazol}$-2+$C_{oxadiazol}$-2′), 150.8 ($C_{pyridin}$-2+$C_{pyridin}$-2'+$C_{pyridin}$-6+$C_{pyridin}$-6′), 144.7 ($C_{pyridin}$-4'+$C_{pyridin}$-4′), 122.6 ($C_{pyridin}$-3+$C_{pyridin}$-3'+$C_{pyridin}$-5+$C_{pyridin}$-5′, 36.3 (*C*a + *C*a'), 30.9 (*C*b). Elemental analysis calcd for $C_{17}H_{14}N_6O_2S_2$ (398.46): C, 51.24; H, 3.54; N, 21.09, found: C, 51.20; H, 3.50; N, 21.05.

2.1.6. 1,3-Bis((5-(p-tolyl)-1,3,4-oxadiazol-2-yl)thio)propane (**9**)

From dibromopropane (202 mg) and **3c** (384 mg). Yield: 662 mg (78%) as white solid; mp: 111–112 °C; IR (KBr, cm^{-1}): ν_{max} 3057 (CH–Ar), 1599 (C=N), 1466 (C–H bending), 1054 (C–*O*–C oxadiazole); ^{1}H NMR (400 MHz, $CDCl_3$): δ 7.89 (d, 4H, J = 9.0 Hz, $H_{arom.}$-2+$H_{arom.}$-2'+$H_{arom.}$-6+$H_{arom.}$-6′), 7.30 (d, 4H, J = 9.0 Hz, $H_{arom.}$-3+$H_{arom.}$-3'+ $H_{arom.}$-5+$H_{arom.}$-5′), 3.48 (t, 2H, J = 7.0 Hz, CH_2-a+CH_2-a'), 2.48 (quin, 4H, J = 6.9 Hz, CH_2-b), 2.43 (s, 6H, 2xAr-*Me*); ^{13}C NMR (400 MHz, $CDCl_3$): δ 166.0 ($C_{oxadiazol}$-5+$C_{oxadiazol}$-5′), 163.4 ($C_{oxadiazol}$-2+$C_{oxadiazol}$-2′), 142.2 ($C_{arom.}$-4+$C_{arom.}$-4′), 129.7 ($C_{arom.}$-2+$C_{arom.}$-2′), 126.6 ($C_{arom.}$-3+ $C_{arom.}$-3′), 120.7 ($C_{arom.}$-1+ $C_{arom.}$-1′), 30.9 (*C*a + *C*a'), 28.7 (*C*b), 21.6 (2xAr-*Me*). Elemental analysis calcd for $C_{21}H_{20}N_4O_2S_2$ (424.54): C, 59.41; H, 4.75; N, 13.20, found: C, 59.31; H, 4.70; N, 13.15.

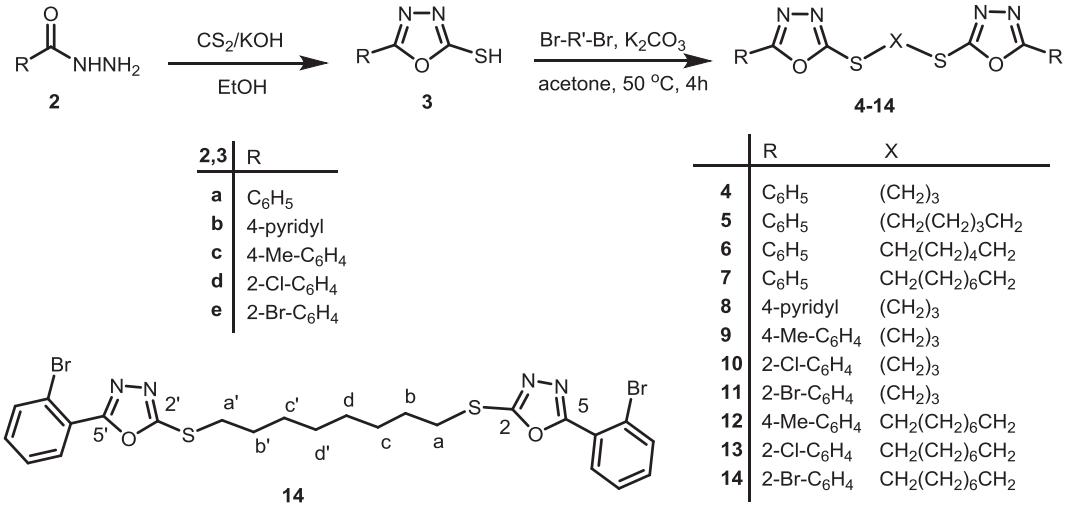

Scheme 1. Synthesis of bis((5-aryl-1,3,4-oxadiazol-2-yl)thio)alkanes (**4**–**14**).

*2.1.7. 1,3-Bis((5-(2-chlorophenyl)-1,3,4-oxadiazol-2-yl)thio) propane (**10**)*

From dibromopropane (202 mg) and **3d** (358 mg). Yield: 679 mg (73%) as white solid; mp: 76–78 °C; IR (KBr, cm^{-1}): ν_{max} 3060 (CH–Ar), 1601 (C=N), 1470 (C–H bending), 1054 (C–*O*–C oxadiazole); ^{1}H NMR (400 MHz, $CDCl_3$): δ 7.96 (dd, 2H, J = 1.8, 7.8 Hz, $H_{arom.}$-6+$H_{arom.}$-6′), 7.57 (m, 4H, $H_{arom.}$-3+$H_{arom.}$-3′), 7.39 (m, 4H, $H_{arom.}$-4+ $H_{arom.}$-4'+$H_{arom.}$-5+$H_{arom.}$-5′), 3.51 (t, 4H, J = 6.9 Hz, CH_2-a+CH_2-a'), 2.52 (quin, 2H, J = 6.9 Hz, CH_2-b); ^{13}C NMR (400 MHz, $CDCl_3$): δ 164.7 ($C_{oxadiazol}$-5+$C_{oxadiazol}$-5′), 164.5 ($C_{oxadiazol}$-2+$C_{oxadiazol}$-2′), 134.6 ($C_{arom.}$-1+$C_{arom.}$-1′), 132.5 ($C_{arom.}$-2+$C_{arom.}$-2′), 131.4, 127.6, 124.9, 121.5 ($C_{arom.}$), 30.9 (*C*a + *C*a'), 28.8 (*C*b'). Elemental analysis calcd for $C_{19}H_{14}Cl_2N_4O_2S_2$ (465.38): C, 49.04; H, 3.03; N, 12.04, found: C, 48.90; H, 3.01; N, 11.85.

*2.1.8. 1,3-Bis((5-(2-bromophenyl)-1,3,4-oxadiazol-2-yl)thio) propane (**11**)*

From dibromopropane (202 mg) and **3e** (514 mg). Yield: 809 mg (73%) as white solid; mp: 89–91 °C; IR (KBr, cm^{-1}): ν_{max} 3061 (CH–Ar), 1605 (C=N), 1460(C–H bending), 1054 (C–*O*–C oxadiazole); ^{1}H NMR (400 MHz, $CDCl_3$): δ 7.91 (dd, 2H, J = 1.8, 7.8 Hz, $H_{arom.}$-3+$H_{arom.}$-3′), 7.66 (dd, 2H, J = 1.2, 7.8 Hz, $H_{arom.}$-6+$H_{arom.}$-6′), 7.49 (m, 2H, $H_{arom.}$-4+$H_{arom.}$-4′), 7.36 (m, 2H, $H_{arom.}$-5+$H_{arom.}$-5′), 3.51 (t, 2H, J = 7.2 Hz, CH_2-a+CH_2-a'), 2.54 (quin, 2H, J = 7.2 Hz, CH_2-b); ^{13}C NMR (400 MHz, $CDCl_3$): δ 164.7 ($C_{oxadiazol}$-5+$C_{oxadiazol}$-5′), 164.5 ($C_{oxadiazol}$-2+$C_{oxadiazol}$-2′), 134.6 ($C_{arom.}$-1+$C_{arom.}$-1′), 132.5 ($C_{arom.}$-3+$C_{arom.}$-3′), 131.4 ($C_{arom.}$-4+$C_{arom.}$-4′), 127.6 ($C_{arom.}$-6+$C_{arom.}$-6′), 124.9 ($C_{arom.}$-5+$C_{arom.}$-5′), 121.5 $C_{arom.}$-2+$C_{arom.}$-2′), 31.0 (*C*a + *C*a'), 28.7 (*C*b). Elemental analysis calcd for $C_{19}H_{14}Br_2N_4O_2S_2$ (554.28): C, 41.07; H, 2.55; N, 10.11, found: C, 41.15; H, 2.50; N, 10.00.

*2.1.9. 1,8-Bis((5-(p-tolyl)-1,3,4-oxadiazol-2-yl)thio)octane (**12**)*

From dibromooctane (272 mg) and **3c** (384 mg). Yield: 702 mg (71%) as white solid; mp: 125–127 °C; IR (KBr, cm^{-1}): ν_{max} 3066 (CH–Ar), 1606 (C=N), 1459 (C–H bending), 1054 (C–*O*–C oxadiazole); ^{1}H NMR (400 MHz, $CDCl_3$): δ 7.88 (d, 4H, J = 8.7 Hz, $H_{arom.}$-2+$H_{arom.}$-2'+$H_{arom.}$-6+$H_{arom.}$-6′), 7.29 (d, 4H, J = 8.7 Hz, $H_{arom.}$-3+$H_{arom.}$-3'+$H_{arom.}$-5+$H_{arom.}$-5′), 3.28 (t, 4H, J = 7.5 Hz, CH_2-a+CH_2-a'), 1.88 (m, 4H, CH_2-b + CH_2-b'), 1.68 (m, 4H, CH_2-c + CH_2-c'), 1.36 (m, 4H, CH_2-d + CH_2-d'), 2.41 (s, 6H, 2xAr-*Me*); ^{13}C NMR (400 MHz, $CDCl_3$): δ 165.5 ($C_{oxadiazol}$-5+$C_{oxadiazol}$-5′), 164.0 ($C_{oxadiazol}$-2+$C_{oxadiazol}$-2′), 142.0 ($C_{arom.}$-4+$C_{arom.}$-4′), 129.6 ($C_{arom.}$-2+$C_{arom.}$-2′), 126.5 ($C_{arom.}$-3+$C_{arom.}$-3′), 120.9 ($C_{arom.}$-1+$C_{arom.}$-1′), 32.5 (*C*a + *C*a'), 29.1 (*C*b + *C*b'), 28.7 (*Cc* + *Cc*'), 28.4 (*C*d + *C*d'), 21.5 (2xAr-*Me*). Elemental analysis calcd for $C_{26}H_{30}N_4O_2S_2$ (494.67): C, 63.03; H, 6.11; N, 11.33, found: C, 63.10; H, 6.08; N, 11.28.

*2.1.10. 1,8-Bis((5-(2-chlorophenyl)-1,3,4-oxadiazol-2-yl)thio) octane (**13**)*

From dibromooctane (272 mg) and **3d** (358 mg). Yield: 750 mg (70%) as white solid; mp: 91–93 °C; IR (KBr, cm^{-1}): ν_{max} 3072 (CH–Ar), 1598 (C=N), 1462 (C–H bending), 1054 (C–*O*–C oxadiazole); ^{1}H NMR (400 MHz, $CDCl_3$): δ 7.92 (dd, 1H, J = 1.8, 7.8 Hz, $H_{arom.}$-6+ $H_{arom.}$-6′), 7.76 (dd, 2H, J = 1.2, 7.8 Hz, $H_{arom.}$-3+ $H_{arom.}$-3′), 7.36 (m, 4H, $H_{arom.}$-4+ $H_{arom.}$-4'+$H_{arom.}$-5+$H_{arom.}$-5′), 3.51 (t, 4H, J = 7.2 Hz, CH_2-a+CH_2-a'), 1.85 (m, 4H, CH_2-b + CH_2-b'), 1.62 (m, 4H, CH_2-c + CH_2-c'), 1.37 (m, 4H, CH_2-d + CH_2-d'); ^{13}C NMR (400 MHz, $CDCl_3$): δ 165.6 ($C_{oxadiazol}$-5+$C_{oxadiazol}$-5′), 164.5 ($C_{oxadiazol}$-2+$C_{oxadiazol}$-2′), 136.5 ($C_{arom.}$-1+$C_{arom.}$-1′), 131.2 ($C_{arom.}$-2+$C_{arom.}$-2′), 130.0, 129.0, 128.5, 127.5 ($C_{arom.}$), 36.5 (*C*a + *C*a'), 30.2 (*C*b + *C*b'), 28.9 (*Cc* + *Cc*'), 28.5 (*C*d + *C*d'). Elemental analysis calcd for $C_{24}H_{24}Cl_2N_4O_2S_2$ (535.51): C, 53.83; H, 4.52; N, 10.46, found: C, 53.75; H, 4.49; N, 10.30.

*2.1.11. 1,8-Bis((5-(2-bromophenyl)-1,3,4-oxadiazol-2-yl)thio) octane (**14**)*

From dibromooctane (272 mg) and **3e** (514 mg). Yield: 899 mg (72%) as white solid; mp: 112–114 °C; IR (KBr, cm^{-1}): ν_{max} (CH–Ar), 1603 (C=N), 1463 (C–H bending), 1054 (C–*O*–C oxadiazole); ^{1}H NMR (400 MHz, $CDCl_3$): δ 7.95 (dd, 2H, J = 1.8, 7.8 Hz, $H_{arom.}$-3+$H_{arom.}$-3′), 7.67 (dd, 2H, J = 1.2, 7.8 Hz, $H_{arom.}$-6+$H_{arom.}$-6′), 7.45 (m, 2H, $H_{arom.}$-4+$H_{arom.}$-4′), 7.39 (m, 2H, $H_{arom.}$-5+$H_{arom.}$-5′), 3.30 (t, 4H, J = 7.1 Hz, CH_2-a+CH_2-a'), 1.83 (CH_2-b + CH_2-b'), 1.64 (m, 4H, CH_2-c + CH_2-c'), 1.36 (m, 4H, CH_2-d + CH_2-d'); ^{13}C NMR (400 MHz, $CDCl_3$): δ 165.6 ($C_{oxadiazol}$-5+$C_{oxadiazol}$-5′), 164.5 ($C_{oxadiazol}$-2+$C_{oxadiazol}$-2′), 139.5 ($C_{arom.}$-1+$C_{arom.}$-1′), 132.2 ($C_{arom.}$-3+$C_{arom.}$-3′), 130.5 ($C_{arom.}$-4+$C_{arom.}$-4′), 129.5 ($C_{arom.}$-6+$C_{arom.}$-6′), 128.5 ($C_{arom.}$-5+$C_{arom.}$-5′), 120.5 ($C_{arom.}$-2+$C_{arom.}$-2′), 36.5 (*C*a + *C*a'), 30.2 (*C*b + *C*b'), 28.9 (*Cc* + *Cc*'), 28.5 (*C*d + *C*d'). Elemental analysis calcd for $C_{24}H_{24}Br_2N_4O_2S_2$ (624.41): C, 46.16; H, 3.87; N, 8.97, found: C, 46.10; H, 3.82; N, 8.92.

2.2. X-ray crystal structure determination

Crystals of compounds **4** and **12** were analyzed by X-ray

crystallography. Selected crystals were coated with paratone 8772 oil and placed on a glass fiber. All measurements were made on Bruker Kappa *APEX*-IICCD diffractometer with graphite monochromated M_o-K_α radiation. The structures were solved by direct methods and refined by using *SHELXL2013* (Sheldrick, 2) [29].

2.3. Computational analysis

DFT studies were performed by using Gaussian 09 [30]. Visualization of molecules at their optimized geometries, FMOs and molecular electrostatic potential surfaces (MEP) were developed with GaussView 05 [31] program package. The X-ray geometry was taken as input for theoretical studies in order to compare the results obtained from theory with experiment. The geometry taken from X-ray crystal was then allowed to completely relax without any symmetry constraints. The optimization of all compounds **4**–**14** was performed at B3LYP (Becke three-parameter Lee–Yang–Parr) exchange-correlation functional [32]. 6-31G (d,p) basis set was used for all atoms (C, N, H, O, S). The frequency calculations confirmed the optimized geometries as a true minimum. Molecular electrostatic potential (MEP) and frontier molecular orbitals (FMOs) analyses were performed at B3LYP/6-31G (d, p) level of DFT.

3. Results and discussions

3.1. Chemistry

The development of novel reagents and antibiotics for combating multidrug resistance bacteria has received significant attention in recent years. Recently, Mandler *et al.* [33] noted that increasing chain length of both the alkyl chain and the linker correlated with increased antimicrobial activity during their synthesis of 4,5-disubstituted-2-aminoimidazole, as the analogue with 5-carbon spacer was most active. Moreover, Yarinich *et al.* [34] reported that a clear structure-activity relationship exists between alkyl chain length of substitutions of 1,4-diazabicyclo [2.2.2] octane tertiary amine sites and antimicrobial activity. Based on these results, we have selected the readily available building blocks aryl-1,3,4-oxadiazole-2-thiols **3a-e** to synthesize new analogues of arylated bis-oxadiazole moieties bearing aliphatic spacers of varying length, aiming to optimize their antimicrobial activity. Thus, treatment of **3a-e**, prepared from the carbohydrazide analogues **2** according to the literature methods, with dibromoalkanes: (alkanes: propane, pentane, hexane, and octane) in acetone and K_2CO_3 at 50 °C afforded, after purification, the bis((5-aryl-1,3,4-oxadiazol-2-yl)thio)alkanes **4**–**14** in 54–80% yield. The synthetic reactions are summarized in Scheme 1.

The structures of **4**–**14** were determined by their IR, ^{1}H, and ^{13}C NMR spectra. In the IR spectra, In the IR spectra, the C=N and C=C absorption are found in the region 1606-1592 cm^{-1}, respectively. The C–H bending and stretching for the target compounds appeared in the region of 1470–1449 and 3072-3055 cm^{-1} respectively. The absence of the absorption band at 2500 cm^{-1} of S–H group was a further support for formation of the desired molecules. The ^{1}H NMR spectra of **4**–**14** were characterized by the presence of additional aromatic protons and carbon atoms, indicative for dimerizarion of the key intermediates **3a-e** *via* the methylene groups as a spacer. The aromatic protons of **4**–**7** appeared as multiplets at the regions δ 8.08–7.28 ppm, while the two doublets at δ 8.70 and 7.91 ppm (J = 3.8 Hz) were assigned to pyridine protons H-2, H-6, and H-3, H-5 (integrated for eight protons), respectively of compound **8**. However, the aromatic protons of **8**–**14** were fully analyzed (*c.f.* Experimental section). The triplets at the regions δ 8.08–7.28 ppm (J ~ 7.5–6.8 Hz) ppm were attributed to CH_2-a, CH_2-a', whereas the multiplets or quintets at the regions δ 2.54–1.66 ppm (J ~ 7.2–6.9 Hz) were assigned to CH_2-b, CH_2-b' of the analogues **4**–**14**. CH_2-c protons of compounds **4**, **5**, and **8**–**10** or CH_2-c, CH_2-c' of compounds **6**, **7**, and **11**–**14** appeared as multiplets at the regions δ 1.70–1.49 ppm. Additionally, CH_2-d, CH_2-d' protons of **7**, and **12**–**14** were resonated as multiplets at the regions δ 1.39–1.36 ppm. In the ^{13}C NMR spectra, C-2, C-2′ atoms of the oxadiazole ring resonated in the range δ 164.7–163.4 ppm, while the C-5, C-5′ signals of the same ring were observed at δ 166.0–164.5 ppm. The resonances at the region δ 142.3–120.5 ppm were assigned to the aromatic carbon atoms of **4**–**8** and **10**–**14**, while the resonances at δ 150.8 and 122.6 ppm were assigned for C-2, C-6 and C-3, C5 of the pyridine moiety of **9**, respectively. Compound **9** showed signal at δ 144.7 ppm assigned for C-4, C-4′ of the pyridine ring. In addition, all the spectra of **4**–**14** showed new signals corresponding to the methylene carbons. The aliphatic carbon atoms (*C*a, *C*a') resonated at the regions δ 36.5–30.9 ppm, while carbon atom (*C*b) of **4**, **8**–**11** appeared at the region δ 30.9–28.7 ppm. Carbon atoms (*C*b, *C*b') of **5**–**7** and **11**–**14** appeared at δ 32.5–29.5 ppm, while carbon atoms (*Cc*, *Cc*') of **6**, **7** and **11**–**14** resonated at the regions δ 29.1–28.7 ppm. The signal at δ 28.5 was attributed to carbon atom (*Cc*) of **5**, whereas carbon atoms (*C*d, *C*d') of **7** and **11**–**14** resonated at δ 28.8–28.5 ppm. The substituents of aromatic residue have been fully identified (*c.f.* Experimental section).

3.2. X-ray crystal structures

Structures of compounds **4** and **12** were unequivocally confirmed by X-ray crystallography. *ORTEP* plots of **4** and **12** are shown in Figs. 1 and 2 while packing pattern is shown in Figs. 3 and 4, respectively. Selected crystal parameters are listed in Table 1. Packing diagram of **4** indicated that the molecule is stabilized by several non-bonding interactions *via* C––N1···N3 and exist as dimer. Compound **4** is not centrosymmetric about its central carbon atom C10. The benzene rings A (C1–C6) and B (C14–C19) are planar with r. m. s. deviation of 0.0035 and 0.0051 Å, respectively. The dihedral angle between rings A and B is 85.05 (9)°. Similarly the 1,3,4-oxadiazole-2-thiol moieties C (C7/C8/N1/N2/O1/S1) and D (C12/C13/N3/N4/O2/S2) are planar with r. m. s. deviation of 0.0048 and 0.0198 Å, respectively. The dihedral angle between C and D is 72.44 (8)°. The dihedral angles between A and C is 14.29 (18)°, whereas the dihedral angle between B and D is 13.55 (17)°, respectively. These dihedral angles gives clear picture that the molecules cannot be centrosymmetric. Further, there is π-π interactions between the centroids of oxadiazole and benzene rings. If Cg1, Cg2, Cg3 and Cg4 are the centroids of (C7/C8/N1/N2/O1), (C12/C13/N3/N4/O2), (C1–C6) and (C14–C9), then the distances between Cg1 … $Cg1^i$ (i = 2 - x, 1 - y, 1 - z), Cg1 … $Cg2^{ii}$ (ii = x, 1/2 - y, 1/2 + Z), Cg1 … $Cg3^i$ and Cg1 … $Cg4^{ii}$ are 3.6271 (13) Å [slippage = 1.609 Å], 3.2334 (13) Å, 3.5683 (13) Å and 3.3431 (13) Å, respectively. Similarly the centroid to centroid distances for Cg3 …

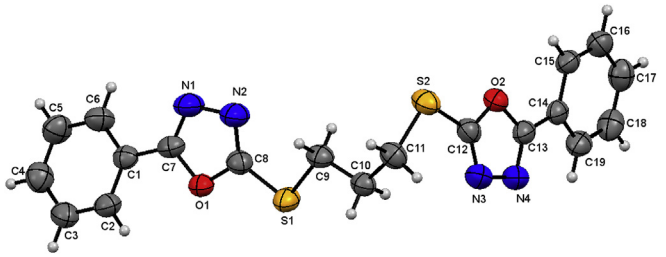

Fig. 1. The molecular structure of **4**, showing 40% probability displacement ellipsoids with atomic numbering. Hydrogen has been omitted for clarity purpose.

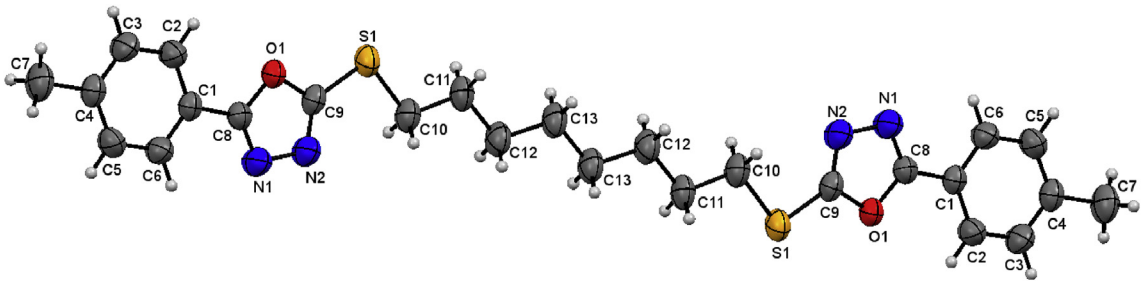

Fig. 2. The molecular structure of **12**, showing 40% probability displacement ellipsoids with atomic numbering. Hydrogen has been omitted for clarity purpose.

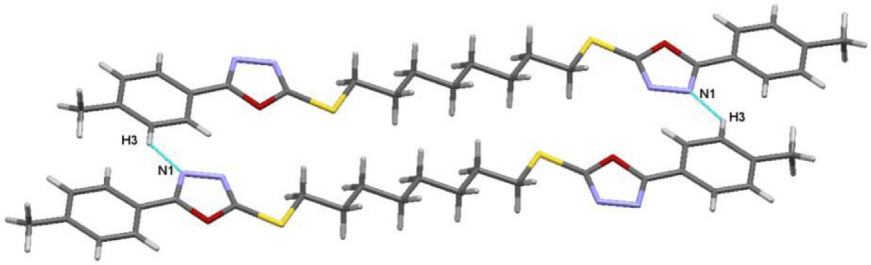

Fig. 3. Packing diagram of **12** showing dimeric interaction *via* C–H–N interactions.

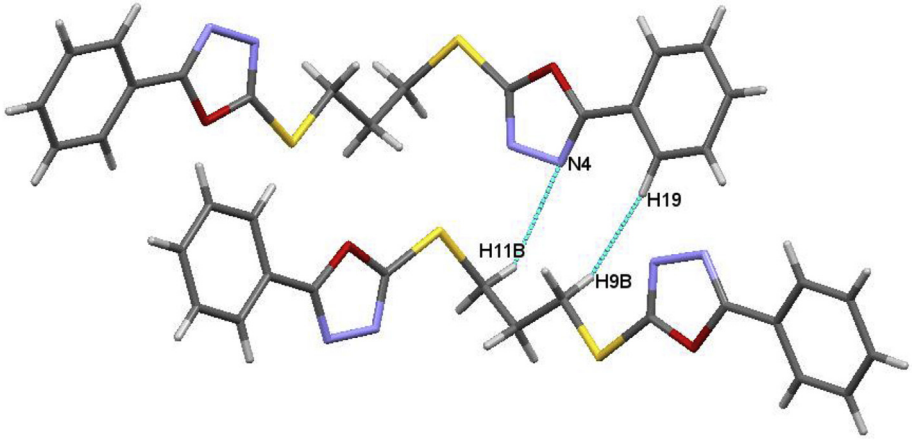

Fig. 4. Packing diagram of **4**, showing dimeric interaction *via* C–H–N and C–H–H–C interactions.

Table 1
Crystallographic data and structure refinement summary for **4** and **12**.

Compd.	**4**	**12**
Formula	$C_{19}H_{16}N_4O_2S_2$	$C_{13}H_{15}N_2OS$
M_r	396.48	247.33
Crystal size (mm)	0.40 × 0.28 × 0.26	0.40 × 0.24 × 0.20
Crystal system	Monoclinic	Triclinic
Space group	$P2_1/c$	P1
Temperature (K)	296	296
Cell constants:		
a (Å)	9.4209 (4)	5.1044 (5)
b (Å)	18.3715 (12)	7.2879 (8)
c (Å)	11.0075 (6)	17.5518 (18)
β (°)	102.073 (3)	84.657 (4)
γ		85.801 (5)
V (Å^3)	1863.00 (18)	643.32 (12)
Z	4	2
μ (mm^{-1})	0.31	0.24
No. Of reflections	4210	2918
No. Of parameters	244	155
$\Delta\rangle_{max}$, $\Delta\rangle_{min}$ (e Å^{-3})	0.24, −0.21	0.21, −0.18

Cg1^{i} (i = 2 - x, 1 - y, 1 - z), Cg3 … Cg3^{iii} (iii = x, 3/2 - y, 1/2 + Z), Cg3 … Cg4^{i} and Cg4 … Cg4^{iv} (iv = 2 - x, -y, 1 - z) are 3.2211 (13) Å, 3.1026 (13) Å, 4.0944 (13) Å and 3.4598 (13) Å [slippage 1.462 Å], respectively. The molecules are mainly stabilized due to these π-π interactions and van der Waals forces.

Crystallographic data have been deposited with the Cambridge Crystallographic Data Centre as supplementary publication no. CCDC-985699 and 992292 for **4** and **12**, respectively. Copies of the data can be obtained free of charge from www.ccdc.cam.ac.uk/data_request/cif.

Similarly compound **12** showed non-bonding interactions and also existed as a dimer *via* C––H––N and C––H––H––C interactions. Compound **12** is centrosymmetric and thus consists of two asymmetric units. In the asymmetric unit of **12**, the tolyl group A (C1–C7), the 1,3,4-oxadiazole-2-thiol moiety B (C8/C9/N1/N2/O1/S1) and the butane group C (C10–C13) are planar with r. m. s. deviation of 0.0179, 0.0041 and 0.0214 Å, respectively. The dihedral angle between A/B, A/C and B/C are 6.17 (9)°, 9.95 (21)° and 8.91

(20)°, respectively. There is π-π interactions between the centroids of oxadiazole Cg1 and benzene rings Cg2, where Cg1 … $Cg1^{i}$ = 3.5147 (7) Å and Cg2 … $Cg2^{i}$ = 3.3939 (8) Å, [i = 1 + x, y, z] with slippage 3.702 and 3.813 Å, respectively. Both molecules **4** and **12** are mainly stabilized due to the π-π interactions and van der Waals forces.

3.3. Computational study

3.3.1. Geometry optimization

In recent years computational methods have got the attention of scientific community because of their wide range applications. The density functional theory (DFT) calculations is one of the abundantly used computational method to investigate the structural properties of compounds [35]. DFT can be applied to investigate the structural parameters, in order to explain the structure activity relationship [36]. The optimized geometries of **4**–**14** are shown in Fig. 5.

The geometries of compounds **4** and **12** were optimized in gas and solvent ($CHCl_3$ was selected because both have excellent solubility in respective solvent) phases. The geometries were optimized in solvent phase for better understaind the geometries in the real system. The solvent effect was studied through CPCM model. The comparative analysis of all important bond lengths and bond angles of **4** and **12** (X-ray and theoretical data) is given in Tables 2 and 3, respectively. From the values narrated in the tables, it is cleared that strong correlation exists between experimental and theoretical (gas as well as solvent phase) data. The difference

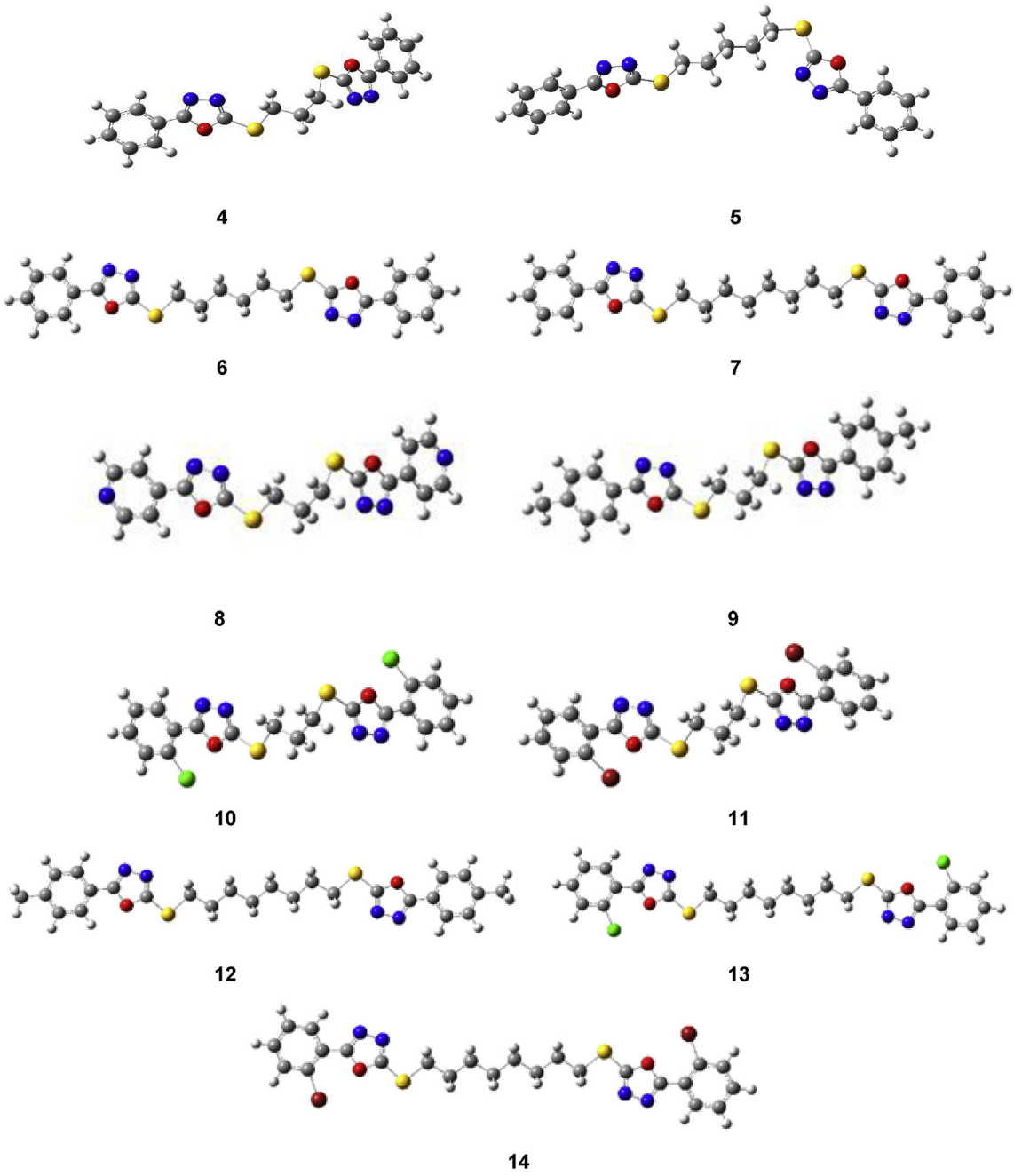

Fig. 5. Optimized geometries of compounds (**4**–**14**) at DFT/B3LYP/6-31G (d, p) level of theory.

Table 2
Comparison of important X-ray and simulated bond lengths [Å] of **4** and **12**, respectively (Atomic labels are with reference *ORTEP* plots, Figs. 1 and 2).

4	Bond lengths (X-ray)	(Calcd.) Gas	Solvent (CHCl3)	**12**	Bond lengths (X-ray)	(Calcd.) Gas	Solvent ($CHCl_3$)
S1–C8	1.72 (18)	1.74	1.74	S1–C9	1.72 (16)	1.74	1.74
S1–C9	1.81 (17)	1.84	1.84	S1–C10	1.80 (18)	1.84	1.84
S2–C12	1.73 (19)	1.75	1.74	O1–C9	1.35 (18)	1.36	1.37
S2–C11	1.81 (18)	1.84	1.84	O1–C8	1.36 (19)	1.37	1.36
O1–C8	1.35 (19)	1.36	1.35	N1–C8	1.28 (2)	1.29	1.30
O1–C7	1.36 (19)	1.37	1.37	N1–N2	1.41 (2)	1.39	1.40
O2–C12	1.36 (2)	1.35	1.36	N2–C9	1.28 (2)	1.29	1.30
O2–C13	1.36 (19)	1.37	1.37	C1–C6	1.38 (2)	1.40	1.40
C5–C6	1.37 (3)	1.39	1.39	C1–C2	1.38 (2)	1.40	1.40
N1–C7	1.28 (2)	1.29	1.29	C1–C8	1.45 (2)	1.45	1.45
N1–N2	1.41 (2)	1.39	1.39	C2–C3	1.38 (2)	1.38	1.38
N2–C8	1.28 (2)	1.29	1.29	C3–C4	1.37 (3)	1.40	1.40
N3–C12	1.28 (2)	1.29	1.30	C4–C5	1.38 (3)	1.39	1.40
N3–N4	1.42 (2)	1.39	1.39	C4–C7	1.50 (2)	1.50	1.50
N4–C13	1.28 (2)	1.29	1.29	C5–C6	1.37 (2)	1.39	1.39
C1–C2	1.38 (2)	1.40	1.40	C10–C11	1.51 (2)	1.52	1.52
C1–C6	1.39 (2)	1.40	1.40	C11–C12	1.51 (3)	1.53	1.53
C1–C7	1.45 (2)	1.45	1.45	C12–C13	1.51 (2)	1.53	1.53
C2–C3	1.37 (3)	1.39	1.39				
C3–C4	1.37 (3)	1.39	1.39				
C4–C5	1.38 (3)	1.39	1.39				
C9–C10	1.51 (2)	1.52	1.53				
C10–C11	1.52 (2)	1.53	1.52				
C13–C14	1.45 (2)	1.45	1.45				
C14–C15	1.39 (2)	1.40	1.40				
C14–C19	1.39 (2)	1.40	1.40				
C15–C16	1.37 (2)	1.39	1.39				
C16–C17	1.37 (3)	1.39	1.39				
C17–C18	1.38 (3)	1.39	1.39				
C18–C19	1.37 (3)	1.39	1.39				

Table 3
Comparison of important X-ray and simulated bond angles [°] of **4** and **12**, respectively (Atomic labels are with reference *ORTEP* plots, Figs. 1 and 2).

4	Bond angles (X-ray)	(Calcd.) Gas	$CHCl_3$	**12**	Bond angles (X-ray)	(Calcd.) Gas	$CHCl_3$
C8–S1–C9	100.2 (8)	98.1	99.4	C9–S1–C10	98.0 (16)	98.5	99.1
C12–S2–C11	100.1 (9)	98.7	99.1	C9–O1–C8	102.0 (12)	102.2	102.7
C8–O1–C7	102.6 (12)	102.2	102.6	C8–N1–N2	106.7 (18)	107.0	107.0
C12–O2–C13	102.7 (13)	102.2	102.6	C9–N2–N1	105.3 (19)	105.7	105.8
C7–N1–N2	106.8 (15)	107.0	107.0	N1 C8 O1	112.2 (13)	111.8	111.5
C8–N2–N1	105.2 (15)	105.7	105.9	N1–C8–C1	127.1 (15)	128.9	129.0
C12–N3–N4	105.7 (14)	105.8	105.7	O1–C8–C1	120.5 (14)	119.2	119.3
C13–N4–N3	106.2 (15)	106.9	107.0	N2–C9–O1	113.5 (14)	113.1	112.7
N1–C7–O1	111.8 (15)	111.8	111.6	N2–C9–S1	128.6 (13)	129.8	130.3
N1–C7–C1	129.3 (16)	128.8	129.1	O1–C9–S1	117.8 (12)	117.0	116.9
O1–C7–C1	118.7 (14)	119.3	119.2	C11 C10 S1	110.11 (14)	109.3	109.4
N2–C8–O1	113.2 (15)	113.1	112.7				
N2–C8–S1	130.3 (14)	129.7	130.6				
O1–C8–S1	116.4 (11)	117.1	116.5				
C10–C9–S1	106.6 (11)	109.0	115.6				
N3–C12–O2	113.0 (16)	113.0	112.8				
N3–C12–S2	131.4 (14)	130.0	130.4				
O2–C12–S2	115.4 (12)	116.8	116.6				
N4–C13–O2	112.1 (16)	111.7	111.6				
N4–C13–C14	129.2 (16)	128.9	129.1				
O2–C13–C14	118.6 (2)	119.2	119.2				
C15–C14–C19	119.4 (17)	119.8	119.8				
C15–C14–C13	120.4 (15)	121.0	120.8				

between the X-ray and theoretical values in important bond lengths of compound **4** is in the range 0.0–0.03 Å for gas as well as solvent phase. The maximum difference between theoretical and experimental bond lengths (0.03 Å) is observed for N3—N4. For compound **12**, the difference between X-ray (experimental) and theoretical (gas and solvent phase) bond lengths is in the range of 0.00–0.04 Å with maximum difference of 0.04 Å for S1–C10. In case of bond angles of both compounds, a similar correlation is observed between theory and experiment. The difference of bond angles between theory and experiment for **4** is in the range of 0.00–2.1° (the maximum difference is for C8–S1–C9). However, in the solvent phase, the values of bond angles are more closer to the X-ray values. Similarly the important bond angles in **12** shows excellent correlation to each other experimentally as well as theoretically. Supp. Table (as Supplementary data) shows the comparison of X-ray and simulated bond lengths [Å] of dimers and trimers in solvent phase of **4** and **12**, respectively.

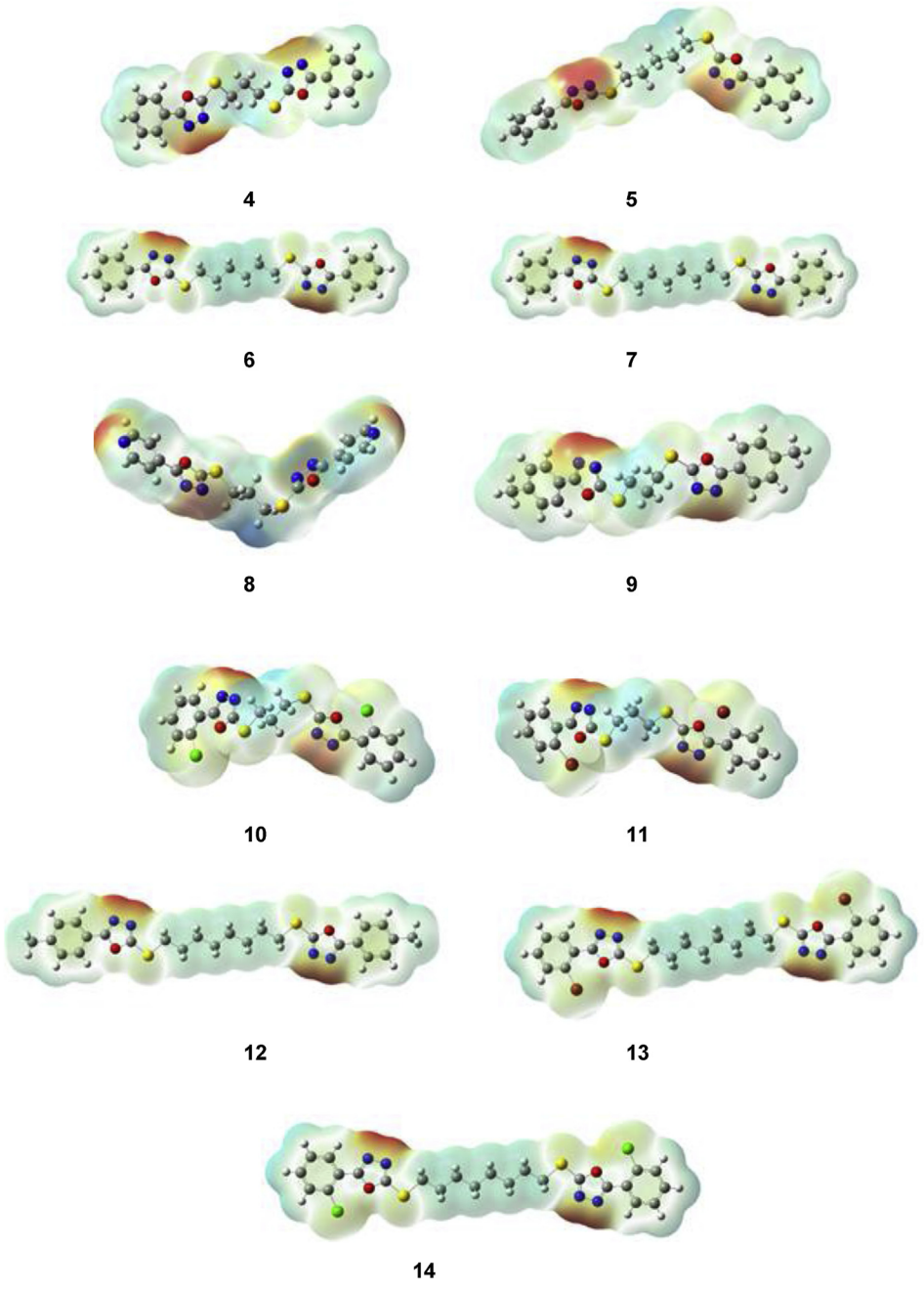

Fig. 6. MEP surfaces of **4**–**14** computed at DFT/B3LYP/6-31 + G (d,p) level.

3.3.2. *Molecular electrostatic potential (MEP)*

The mapping of the electrostatic potential is a famous approach because it plays a key role in the initial steps of biological as well as noncovalent interactions [37]. MEP *i.e.* V(r), at a given point r (x, y, z) of any compound, is the interaction energy between the electrical charges generated by atomic particles at distance (r). Mathematically, MEP can be described by using the following equation:

$$V(r) = \sum \frac{Z_A}{|R_A - r|} - \int \frac{\rho(r')}{|r' - r|} dr'$$

where Z_A is the charge on nucleus A, located at R_A and $\rho(r)$ is the electronic density function for the molecule.

Table 4
ESP values of compounds **4**–**14**.

Compd.	-ve potential (a. u.)	+ve potential (a. u.)
4	−0.05245	0.05245
5	−0.05347	0.05347
6	−0.05226	0.05227
7	−0.05271	0.05271
8	−0.04573	0.04573
9	−0.05437	0.05437
10	−0.04907	0.04907
11	−0.04970	0.04970
12	−0.05447	0.05447
13	−0.04924	0.04924
14	−0.04919	0.04919

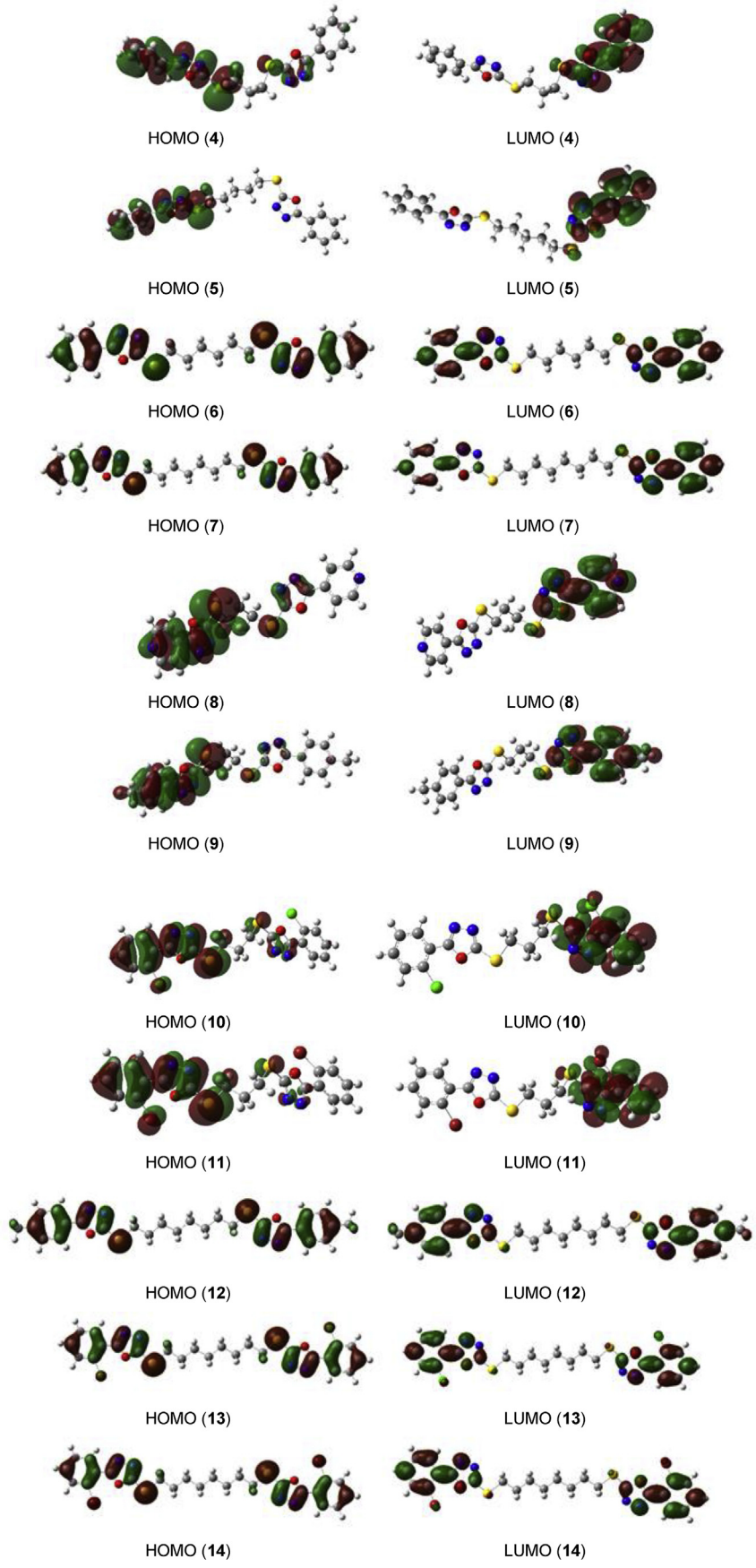

Fig. 7. HOMO-LUMO surfaces of **4**–**14.**

Table 5
HOMO and LUMO energies along with HOMO-LUMO energy gap of **4**–**14**.

Compd.	HOMO (a. u.)	LUMO (a. u.)	HOMO-LUMO (ΔE) eV
4	−0.22474	−0.05195	4.69
5	−0.22349	−0.05046	4.70
6	−0.22498	−0.04856	4.79
7	−0.22398	−0.04788	4.78
8	−0.24139	−0.07305	4.57
9	−0.21979	−0.04797	4.67
10	−0.22759	−0.06038	4.54
11	−0.22782	−0.05825	4.61
12	−0.21936	−0.04424	4.76
13	−0.22666	−0.05666	4.62
14	−0.22698	−0.05668	4.63

The electrostatic potential values at the surfaces are distinguished by the appearance of colors. The electronegative potential is represented by red color and the electropositive potential is represented by blue color. The potential decreases by the following increasing order: red < orange < yellow < green < blue. To predict the electrophilic and nucleophilic sites of **4**–**14**, molecular electrostatic potential (MEP) was calculated at the B3LYP/6-31 + G (d,p) level of DFT by using the optimized geometries. Fig. 6 shows the electrostatic potential surfaces of **4**–**14** and values are summarized in Table 4.

Fig. 6 demonstrated that the negative regions of V(r) related to electrophilic reactivity is located on the oxadiazole ring of the analogues **4**–**14**. Moreover, ESP analysis revealed that these derivatives are nucleophilic in nature and have ability to react with electrophiles. Compound **8** has minimum dispersion of ESP, ranged from −0.04573 a. u. to 0.04573 a. u, which illustrates that **8** is less polarized as compared to others. Additionally, **12** has highest dispersion of ESP values, ranged from −0.05447 a. u. to 0.05447 a. u., and to be the most polarized among all compounds.

3.3.3. *Frontier molecular orbitals (FMOs) analysis*

The FMOs participate in defining the optical and chemical properties of substrates [38]. The FMOs can act as donor and acceptor orbitals [39], respectively. Energy gap between HOMO and LUMO gives an idea about the kinetic stability and conductivity as well. Frontier orbital analysis of **4**–**14** was carried at the same level of DFT as used for energy optimization of structures. The HOMO and LUMO surfaces are shown in Fig. 7, whereas their corresponding energies along with energy difference are given in Table 5. Since **4**–**14** bear the bis((5-aryl-1,3,4-oxadiazol-2-yl)thio) backbone with various aryl substituents and spacers, therefore the FMOs are concentrated on the same thioxadiazol moiety. All compounds revealed almost the similar HOMO-LUMO energy difference, because each compound has almost similar chromophoric group as well as π electronic cloud (individual values are shown in Table 5).

4. Antimicrobial activity

Compounds **4**–**14** were tested for their antibacterial activity against *S. typhimurium, M. luteus* and *B. bronchiseptica* on nutrient agar plates at 37 °C for 24 h using cefixime as a reference drug. The compounds were also screened for their antifungal activity against three different strains; *Aspergilus niger, Mucor species,* and *Aspergilus flavus* using terbinafine as a standard drug. Fungi cultures were grown on potato dextrose agar medium at 25 °C for 72 h.

Examination of the antibacterial and antifungal screening data of our new compounds (Table 6) revealed that all the tested compounds displayed significant to moderate activity against the tested bacteria and fungi compared to the reference drugs. We noted that the substituents of the aryl groups displayed significant inhibitory activity, meanwhile activity was only slightly affected by the length of methylene groups (as spacer) being located between the 1,3,4-oxadiazole moiety, as noted by Mandler as his group. However, compounds **9**, **12** and **14** having 4-methyl- and 4-bromophenyl groups showed better activity against *S. typhimurium, M. Luteus,* and *B. septic* than the corresponding derivatives with phenyl or 4-chlorophenyl residues at C-5 of 1,3,4-oxadiazole moiety. Similarly, **9** and **12** exhibited better antifungal activity against *A. niger*, *Mucor sp.* and *A. flavus,* while **8** having 4-pyridyl moiety possessed the highest antifungal activity against *Mucor sp.* than those of other analogues of the series.

5. Conclusion

The work described in this paper involved the synthesis, crystal structures, DFT studies and antimicrobial assay of some designed bis((5-aryl-1,3,4-oxadiazol-2-yl)thio)alkanes. All synthesized compounds were characterized. Molecular structures of **4** and **12** have been determined by single crystal X-ray analysis. The DFT studies were performed to investigate the structural properties. Geometries of **4**–**14** were optimized at B3LYP/6-31 + G (d,p) level and used for further investigations of ESP and FMOs analysis. The molecular electrostatic potential investigations revealed that all compounds are nucleophilic in nature and electronegative region was spreading mainly on the oxadiazole ring. Compound **8** showed a minimum value of ESP ranged from −0.04573 a. u. to 0.04573 a. u, and was less polarized, whereas **12** showed a highest value, ranged

Table 6
Antimicrobial activities of **4**–**14**.

Compd.	Bacterial strain			Fungal strain		
	S.typhimurium	*M. Luteus*	*B. septica*	*A. niger*	*Mucor sp.*	*A. flavus*
4	9.5 ± 0.8	7.5 ± 0.4	8.0 ± 0.4	10.0 ± 1	11.5 ± 1	9.5 ± 0.3
5	8.0 ± 0.6	9.0 ± 0.3	8.0 ± 0.3	11.5 ± 1	nd	13.5 ± 1
6	8.5 ± 0.4	9.5 ± 0.4	7.5 ± 0.3	9.5 ± 0.4	10.5 ± 1	12.5 ± 1
7	7.5 ± 0.3	8.0 ± 0.4	8.5 ± 0.2	12.0 ± 1	11.5 ± 1	9.5 ± 0.4
8	11.5 ± 1	8.5 ± 0.3	9.0 ± 0.4	15.0 ± 1	15.5 ± 1	14.0 ± 1
9	14.0 ± 1	12.5 ± 1	10.5 ± 1	19.0 ± 1	14.5 ± 1	15.0 ± 1
10	11.0 ± 1	8.5 ± 0.4	7.5 ± 0.3	15.0 ± 1	13.3 ± 1	14.5 ± 1
11	9.0 ± 0.3	8.8 ± 0.4	7.5 ± 0.3	13.0 ± 1	12.5 ± 1	11.5 ± 1
12	12.0 ± 1	13 ± 1	10 ± 1	18.5 ± 1	16.5 ± 1	12.5 ± 1
13	8.5 ± 0.3	nd	7.5 ± 0.4	12.0 ± 1	10.5 ± 1	9.0 ± 0.3
14	13.0 ± 1	10.0 ± 1	11.5 ± 1	15.5 ± 1	11.5 ± 1	10.5 ± 1
Cefixime	22.0 ± 1.15	15 ± 1.52	19 ± 1.52	–	–	–
Terbinafine	–	–	–	30 ± 1.0	28 ± 1.52	33 ± 1.52

nd: not determined.

from −0.05447 a. u. to 0.05447 a. u., and was the most polarized among all synthesized analogues. Frontier molecular orbital analysis showed that band gap for **9** is 5.97 eV, which reflects that **9** is kinetically more stable and less reactive. The synthesized compounds were tested against three different bacterial and three different fungal strains, where most of the compounds exhibited moderate to good activity.

Acknowledgements

Financial support for this work by Higher Education Commission of Pakistan (HEC) and UoAJK is gratefully acknowledged.

Appendix A. Supplementary data

Supplementary data related to this article can be found at https://doi.org/10.1016/j.molstruc.2017.11.011.

References

[1] J. Sun, J.A. Makawana, H.L. Zhu, 1,3,4-oxadiazole derivatives as potential biological agents, Mini Rev. Med. Chem. 13 (2013) 1725–1743 (review).
[2] A. Vaidya, S. Jain, P. Jain, P. Jain, N. Tiwari, R. Jain, R. Jain, A.K. Jain, R.K. Agrawal, Synthesis and biological activities of oxadiazole derivatives: a review, Mini Rev. Med. Chem. 16 (2016) 825–845 (review).
[3] A. Aboraia, H.M.A. Rahman, N. Mahfuz, A. Mohmoud, E.L. Gendy, Novel 5-(2-hydroxyphenyl)-3-substituted-2,3-dihydro-1,3,4-oxadiazole-2-thione derivatives: promising anticancer agents, Bioorg. Med. Chem. 14 (2006) 1236–1246.
[4] Y. Luo, Z.J. Liu, G. Chen, J. Shi, J.R. Li, H.L. Zhu, 1,3,4-Oxadiazole derivatives as potential antitumor agents: discovery, optimization and biological activity valuation, MedChemComm 7 (2016) 263–271.
[5] F.S. Savariz, A.S.N. Formagio, V.A. Barbosa, M.A. Foglio, J.E. Carvalho, M.C.T. Duarte, B.P.D. Filho, M.H. Sarragiotto, Synthesis, antitumor and antimicrobial activity of novel 1-substituted phenyl-3-[3-alkylamino(methyl)-2-thioxo-1,3,4-oxadiazol-5-yl]β-carboline derivatives, J. Braz. Chem. Soc. 21 (2010) 288–298.
[6] L.V.G. Nargund, G.R.N. Reddy, V. Hariprasad, Anti-inflammatory activity of substituted 1,3,4-oxadiazoles, J. Pharm. Sci. 83 (1994) 246–248.
[7] R.V. Shingalapur, K.M. Hosamani, R.S. Keri, M. H, Derivatives of benzimidazole pharmacophore: synthesis, anticonvulsant, antidiabetic and DNA cleavage studies, Eur. J. Med. Chem. 45 (2010) 1753–1759.
[8] S.A. Khanum, S. Shashikanth, S. Umesh, R. Kavitha, Synthesis and antimicrobial study of novel heterocyclic compounds from hydroxybenzophenones, Eur. J. Med. Chem. 40 (2005) 1156–1162.
[9] C.S. de Oliveira, B.F. Lira, J.M. Barbosa-Filho, J.G.F. Lorenzo, P.F. de Athayde-Filho, Synthetic approaches and pharmacological activity of 1,3,4-oxadiazoles: a review of the lLiterature from 2000–2012, Molecules 17 (2012) 10192–10231.
[10] G. Sahin, E. Palaska, M. Ekizoglu, M. Ozalp, Synthesis and antimicrobial activity of some 1,3,4-oxadiazole derivatives, IL Farm. 57 (2002) 539–542.
[11] G.R. Bankar, K. Nandakumar, P.G. Nayak, A. Thakur, M.R. Chamallamudi, G.K. Nampurath, Vasorelaxant effect in rat aortic rings through calcium channel blockage: a preliminary in vitro assessment of a 1,3,4-oxadiazole derivative, Chem. Biol. Interact. 181 (2009) 377–382.
[12] H. Rajak, R. Deshmukh, R. Veerasamy, A.K. Sharma, P. Mishra, M.D. Kharya, Novel semicarbazones based 2,5-disubstituted-1,3,4-oxadiazoles: one more step towards establishing four binding site pharmacophoric model hypothesis for anticonvulsant activity, Bioorg. Med. Chem. Lett. 20 (2010) 4168–4172.
[13] A. Zarghi, S.A. Tabatabai, M. Faizi, A. Ahadian, P. Navabi, V. Zanganeh, A. Shafiee, Synthesis and anticonvulsant activity of new 2-substituted-5-(2-benzyloxyphenyl)-1,3,4-oxadiazoles, Bioorg. Chem. Lett. 15 (2005) 1863–1865.
[14] S.J. Gilani, S.A. Khan, N. Siddiqui, Synthesis and pharmacological evaluation of condensed heterocyclic 6-substituted 1,2,4-triazolo-[3,4-b]-1,3,4-thiadiazole and 1,3,4-oxadiazole derivatives of isoniazid, Bioorg. Med. Chem. Lett. 20 (2010) 4762–4765.
[15] M. Llinàs-Brunet, M.D. Bailey, G. Bolger, C. Brochu, A.-M. Faucher, J.M. Ferland, M. Garneau, E. Ghiro, V. Gorys, C. Grand-Maître, Structure-activity study on a novel series of macrocyclic inhibitors of the hepatitis C virus NS3 protease leading to the discovery of BILN 2061, J. Med. Chem. 47 (2004) 1605–1608.
[16] B. Johns, J.G. Weatherhead, S.H. Allen, J.B. Thompson, E.P. Garvey, S.A. Foster, J.L. Jeffrey, W.H. Miller, 1,3,4-Oxadiazole substituted naphthyridines as HIV-1 integrase inhibitors. Part 2: SAR of the C5 position, Bioorg. Med. Chem. Lett. 19 (2009) 1807–1810.
[17] M. Zareef, R. Iqbal, N.A. Al-Masoudi, J.H. Zaidi, M. Arfan, Microwave-assisted synthesis and anti-HIV activity of new benzenesulfonamides bearing 2,5-disubstituted-1,3,4-oxadiazole moiety, Heteroat. Chem. 18 (2007) 425–431.
[18] R. Iqbal, M. Zareef, S. Ahmed, J.H. Zaidi, M. Arfan, M. Shafique, N.A. Al-Masoudi, Synthesis, antimicrobial and anti-HIV activity of some novel benzenesulfonamides bearing 2,5-disubstituted-1,3,4-oxadiazole moiety, J. Chin. Chem. Soc. 53 (2006) 689–696.
[19] Z. Temesgen, D.S. Siraj, Raltegravir: first in class HIV integrase inhibitor, Ther. Clin. Risk Manag. 4 (2008) 493–500.
[20] D. Leung, W. Du, C. Hardouin, H. Cheng, I. Hwang, B.F. Cravatt, D.L. Boger, Discovery of an exceptionally potent and selective class of fatty acid amide hydrolase inhibitors enlisting proteome-wide selectivity screening: concurrent optimization of enzyme inhibitor potency and selectivity, Bioorg. Med. Chem. Lett. 15 (2005) 1423–1428.
[21] Y. Ducharme, M. Blouin, C. Brideau, A. Châteauneuf, Y. Gareau, E.L. Grimm, H. Juteau, S. Laliberté, B. MacKay, F. Massé, et al., The discovery of setileuton, a potent and selective 5-lipoxygenase inhibitor, Med. Chem. Lett. 1 (2010) 170–174.
[22] F. Gosselin, R.A. Britton, I.W. Davies, S.J. Dolman, D. Gauvreau, R.S. Hoerrner, G. Hughes, J. Janey, S. Lau, C. Molinaro, et al., A practical synthesis of 5-lipoxygenase inhibitor MK-0633, J. Org. Chem. 75 (2010) 4154–4160.
[23] Q.R. Du, D.D. Li, Y.Z. Pi, J.R. Li, J. Sun, F. Fang, W.Q. Zhong, H.B. Gong, H.L. Zhu, Novel 1,3,4-oxadiazole thioether derivatives targeting thymidylate synthase as dual anticancer/antimicrobial agents, Bioorg. Med. Chem. 21 (2013) 2286–2297.
[24] K. Liu, X. Lu, H.J. Zhang, J. Sun, H.-L. Zhu, Synthesis, molecular modeling and biological evaluation of 2-(benzylthio)-5-aryloxadiazole derivatives as anti-tumor agents, Eur. J. Med. Chem. 47 (2012) 473–478.
[25] M. Zahid, K.A. Yasin, T. Akhtar, N.H. Rama, S. Hameed, N.A. Al-Masoudi, R. Loddo, P. La Colla, Synthesis and in vitro antiproliferative activity of new adamantylthiazolyl-1,3,4-oxadiazoles, Ark. xi (2009) 85–93.
[26] F. Macaev, Z. Ribkovskaia, S. Pogrebnoi, V. Boldescu, G. Rusu, et al., Bioorg. Med. Chem. 19 (2011) 6792–6807.
[27] H.H. Fox, Synthetic tuberculostats. II. Amino- and hydroxyl-pyridine carboxylic acid derivatives, J. Org. Chem. 17 (1952) 542–546.
[28] M. Zareef, R. Iqbal, N.G. De Dominguez, J. Rodrigues, J.H. Zaidi, M. Arfan, C.T. Supuran, Synthesis and antimalarial activity of novel chiral and achiral benzenesulfonamides bearing 1, 3, 4-oxadiazole moieties, J. Enzyme Inhib. Med. Chem. 22 (2007) 301–308.
[29] G.M. Sheldrick, Crystal structure refinement with *SHELXL*, Acta Crystallogr. C Struct. Chem. 71 (2015) 3–8.
[30] M.J. Frisch, G.W. Trucks, H.B. Schlegel, G.F. Scuseria, M.A. Robb, J.R. Cheeseman, G. Scalmani, V. Barone, B. Mennucci, G.A. Petersson, et al., Gaussian 09, Revision B.01, Gaussian Inc., Wallingford, CT, 2010.
[31] A. Frisch, A.B. Nielson, A.J. Holder, GaussView User Manuual, Gaussian Inc, Pittsburgh, P. A., 2005.
[32] R.J. Magyar, S. Tretiak, Dependence of spurious charge-transfer excited states on orbital exchange in TDDFT: Large molecules and clusters, J. Chem. Theor. Comput. 3 (2007) 976–987.
[33] Z. Su, S.A. Rogers, W.S. McCall, A.C. Smith, S. Ravishankar, T. Mullikin, C. Melander, A nitroenolate approach to the synthesis of 4,5-disubstituted-2-aminoimidazoles. Pilot library assembly and screening for antibiotic and antibiofilm activity, Org. Biomol. Chem. 8 (2010) 2814–2822.
[34] L.A. Yarinich, E.A. Burakova, B.A. Zakharov, E.V. Boldyreva, I.N. Babkina, N.V. Tikunova, V.N. Silnikov, Synthesis and structure-activity relationship of novel 1,4-diazabicyclo[2.2.2]octane derivatives as potent antimicrobial agents, Eur. J. Med. Chem. 95 (2015) 563–573.
[35] T. van Mourik, M. Bühl, M.-P. Gaigeot, Density functional theory across chemistry, physics and biology, Philos. Trans. A Math. Phys. Eng. Sci. 372 (2014) 20120488.
[36] S. Pan, A. Gupta, D.R. Roy, R.K. Sharma, V. Subramanian, A. Mitra, P.K. Chattaraj, Chapter 6. Application of conceptual density functional theory in developing QSAR models and their usefulness in the prediction of biological activity and toxicity of molecules, in: G.A. Mercader, P.R. Duchowicz, P.M. Sivakumar (Eds.), Chemometrics Applications and Research: QSAR in Medicinal Chemistry, Apple Academic Press, New Jersey, USA, 2016, pp. 183–214.
[37] P.W. Kenny, Hydrogen bonding, electrostatic potential, and molecular design, J. Chem. Inf. Model 49 (2009) 1234–1244.
[38] I. Fleming (Ed.), Frontier Orbitals and Organic Chemical Reactions, 1st. ed., Wiley, London, UK, 1978, pp. 879–880.
[39] E. Kavitha, N. Sandaraganesan, S. Sebastian, Molecular structure, vibrational spectroscopic and HOMO, LUMO studies of 4-nitroaniline by density functional method, Ind. J. Pure Appl. Phys. 48 (2010) 20–30.